1. Bogdan FABIAŃSKI[1], 2. Tomasz PAJCHROWSKI[1], 3. Krzysztof ZAWIRSKI[2]

Poznan University of Technology – Institute of Robotics and Machine Intelligence (1); Academy of Applied Sciences in Pila (2)
ORCID: 1.0000-0001-5852-8674; 2.0000-0002-0002-7161; 3.0000-0003-4401-5880

doi:10.15199/48.2024.11.11

Electronic system and signal processing in torque-meter interface of switched reluctance motor drive laboratory test bench

Abstract. *The article aims to present – from a functional point of view – the key solutions of an automated laboratory stand for testing a switched reluctance motor drive. Particular emphasis was placed on one of the proprietary modules of this stand: the dedicated interface of the FUTEK TRS705 torque meter. In this respect, the physical layer and the most important algorithms are discussed. The concept of building a research test bench that will be able to collect information about the basic relationships of a given specimen in an automated and – at the same time – in precise manner is important since fundamental phenomena: generation of electromagnetic torque and an electromotive force are characterized by significant nonlinearities that must be taken into account in the motor models. Hence the issues presented in the article (precise, open torque meter interface) can be considered and useful in a much broader (generic) context, constituting a contribution to solutions in electric drive. The presented methods and system solutions were verified experimentally along with the final presentation of the results of the station operation.*

Streszczenie. *Artykuł ma na celu przedstawienie -- z funkcjonalnego punktu widzenia -- kluczowych rozwiązań zautomatyzowanego stanowiska laboratoryjnego do badania silnika reluktancyjnego przełączalnego. Szczególny nacisk położono na jeden z autorskich modułów tego stanowiska tj. dedykowany interfejs momentomierza przelotowego marki FUTEK TRS705. W tym zakresie omówiono warstwę fizyczną, jak i najważniejsze algorytmy zaimplementowane w programie systemu wbudowanego. Koncepcja opisywanej budowy stanowiska badawczego, które w sposób zautomatyzowany i zarazem precyzyjny będzie mogło zebrać informacje o podstawowych relacjach danego egzemplarza silnika jest bardzo istotna z perspektywy rozwoju algorytmów sterowania -- w szczególności tych wykorzystujących model referencyjny. Fundamentalne zjawiska: generowania momentu elektromagnetycznego oraz wytwarzania siły elektromotorycznej charakteryzują się w silniku SRM istotnymi nieliniowościami, które powinny być uwzględnione w jego modelach obwodowych. Stąd, przedstawione w artykule zagadnienia mogą być rozpatrywane i użyteczne w znacznie szerszym kontekście. Co istotne, przedstawione metody i rozwiązania układowe zweryfikowano eksperymentalnie wraz z końcowym przedstawieniem rezultatów działania stanowiska. (**Układ elektroniczny i przetwarzanie sygnału w interfejsie miernika momentu obrotowego w stanowisku badawczym laboratoryjnym napędu silnika reluktancyjnego prz**ełączanego)

Keywords: electric drive, SRM, laboratory test bench, torque meter interface, electronic design, signal processing
Słowa kluczowe: napęd elektryczny, SRM, stanowisko badawcze, interfejs momentomierza, przetwarzanie sygnałów

Introduction

Control algorithms in electric drives, regardless of the class of the solution, always refer to the structure/parameters of the control object itself. This knowledge is most often reflected in the parameters/structure of the control algorithms themselves - hence it may be more or less detailed (taking into account more/less precisely the nature of the object). Assuming the task of detecting damage in the drive and then working in these conditions, the algorithms should show an appropriate level of sensitivity. Good convergence of the reference model (that is the basis for the development of the control system) means the system more likely to work effectively in real conditions.

Hence, the task set in the described work is to obtain the possibility of examining whether precise measurement of the motor response in the form of the generated electromagnetic torque T_p in the two-dimensional functional space of the phase current measurement range i_p and the shaft position angle θ_p will be sufficient to define parametric, model nonlinear functions constituting the basis for the developed:

- sensorless control,
- fault detection algorithms,
- control in fault conditions.

It is assumed that it will be possible to directly or indirectly solve the formulas defining the model in related tasks:

- selection of the motor windings excitation angles,
- calculation of the required value of the phase current for a given value of the electromagnetic torque,

according to the criteria:

- minimizing torque ripples (a general task for the SRM motor drive control system),
- maximizing the generated motor torque while limiting the winding current (a special task for operation in fault conditions).

Based on the operation of the electric motor, the purpose of which is (of considerable importance in the modern world) converting electrical energy into mechanical one is characterized by two quantities:

- electromagnetic torque T_e,
- electromotive force ε.

These quantities are strongly interconnected, including the operation of the motor in accordance with the principle of conservation of energy. The nonlinearities of the energy conversion process inherent in the switched reluctance motor (SRM) contribute to the complexity of the formulas describing its mathematical model [1],[2],[3]. For control purposes, this model is most often considered in the class of circuit equations – the model viewed from the perspective of the power terminal circuit (the control signal, which is most often the voltage applied to the motor phase winding). To explain these basic relationships, the fundamental voltage equation of the motor phase winding will be introduced:

$$U_p = i_p R_p + \frac{d\Psi_p}{dt} \quad (1)$$

where: p (−) – motor winding number, U_p (V) – applied voltage, i_p (A) – current of the p-number phase winding, R_p(Ω) – phase resistance, Ψ_p (Wb) – associated magnetic flux, t (s) – time.

Assuming (which is typical for an SRM motor) that the associated flux of the motor phase depends both on the

angle of the shaft relative to the winding θ_p and on the value of the phase current i_p, i.e.:

$$\Psi_p = f(\theta_p, i_p) \tag{2}$$

the equation (1) takes form:

$$U_p = i_p R_p + \frac{d\Psi_p(i_p,\theta_p)}{dt} . \tag{3}$$

After expansion, the second component of the above sum:

$$\frac{d\Psi_p(i_p,\theta_p)}{dt} = \frac{\partial\Psi_p(i_p,\theta_p)}{\partial i_p}\frac{di_p}{dt} + \frac{\partial\Psi_p(i_p,\theta_p)}{\partial\theta_p}\frac{d\theta_p}{dt} , \tag{4}$$

is the reactive component (due to electromagnetic induction) of the motor winding voltage equation. Taking into account in the definition of the flux a parameter that describes the associated phenomena of the magnetic field for the circuit equation (phase winding inductance L_p):

$$\Psi_p(\theta_p, i_p) = L_p(\theta_p, i_p) i_p. \tag{5}$$

The notation of equation 5 indicates that the inductance of the motor phase winding depends not only on the angle of the shaft position (prominent poles of the rotor and stator cause a change in the magnetic permeability when the rotor is moving, so the value of magnetic induction B at the same forced current), but also on the value of the phase current itself taking into account the phenomenon of magnetic field saturation (non-linearity of the relationship $B=f(H)$). The adopted definition of the winding associated flux (Ψ_p) in the motor model affects its accuracy, but also – on the other hand – the computational complexity in control tasks.

Hence, simplified relations are sometimes adopted. In general, approaches to switched reluctance motor modeling can be reduced into three categories:
a) ignoring the phenomenon of saturation of the magnetic circuit [2],[1]:

$$\Psi_p(\theta_p, i_p) = L_p(\theta_p) i_p , \tag{6}$$

b) - with a simplified approach to saturation modeling [4],[5],[6]:

$$\Psi_p(\theta_p, i_p) = L_p(\theta_p) F_{sat}(i_p) , \tag{7}$$

c) - with accurate saturation modeling [7],[8],[9]:

$$\Psi_p(\theta_p, i_p) = L_p(\theta_p, i_p) i_p . \tag{8}$$

The model solutions for these different representations can therefore be reduced - in simple terms - to a computational complexity of the order of:
a) N,
b) $2N$,
c) N^2.

However, in each case, it is important to define nonlinear relations (at least $L_p(\theta_p)$) allowing for obtaining a possibly convergent model. A methodical approach to establishing convergence in a computer environment first requires establishing (in this context) the so-called reference model resulting from a thorough examination of the relationships existing in a real motor. Due to the discussed coupled nonlinearities, such validation requires an appropriate hardware layer to achieve precision and measurements at many different operating points.

Performing such a task manually would be fraught with a high risk of gross error (e.g. error in determining the position) and would be time-consuming. Hence the idea of constructing a dedicated research station in which the entire process is automated and the time of aggregation of measurement data and their processing is reduced to a minimum.

The article places particular emphasis on one of the stand's modules - the proprietary interface of the FUTEK TRS705 torque meter [10]. The essence of this module is reflected in the fact that direct measurement of the torque produced by the motor is a key functionality from the perspective of a previously defined goal. Additionally, it enables experimental verification of the resulting quality of the implemented control (in the context of the task of minimizing ripples or maximizing the generated torque in the angular distribution).

Starting from the formula describing the electromagnetic torque generated in the motor from a given phase p:

$$T_p = \frac{dE_c}{d\theta} , \tag{9}$$

related to the key element of the model, i.e. the adopted formula describing the magnetic flux:

$$E_c(\theta_p, i_p) = \int_{\tau=0}^{i_p} \Psi_p(\theta_p, i_p) d\tau , \tag{10}$$

it is obtained:

$$T_p(\theta_p, i_p) = \frac{d\int_{\tau=0}^{i_p} \Psi_p(\theta_p, i_p) d\tau}{d\theta} . \tag{11}$$

Hence, with direct measurement of the torque as a function of the position angle and the band current, it is possible to determine the variability of the reference inductance. Taking into account (5) in (11) and making the appropriate transformation:

$$\frac{dL_p(\theta_p,i_p)}{d\theta} = \frac{2T_p(\theta_p,i_p)}{i_p^2} \tag{12}$$

without the need to use field models to complete the description of characteristic relationships (as in publications: [8],[9]).

To sum up and bearing in mind the above explanations, the scientific goal of the original construction of the experimental test bench will be to verify the structure and definition of model formulas and to verify the thesis about the possibility of implementing complex control (e.g. assuming minimization of torque ripples) using analytical transformations of the concurrently calculated **reference model** (understood here in the context of the drive control task).

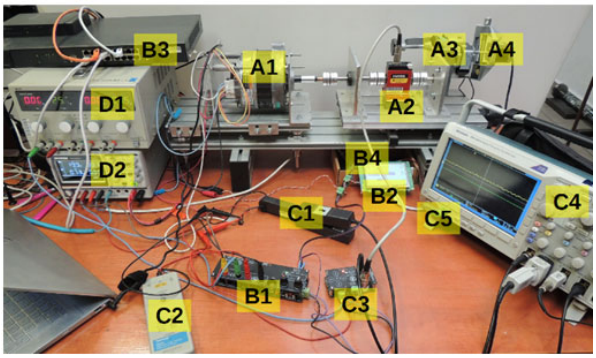

Fig. 1. Picture of the experimental test bench

Structure of the experimental test bench

The task of experimental verification of the developed structures of object models and control algorithms in a switched reluctance motor drive is possible at the station presented in Figure 1. The structure of the experimental set can be divided into four main sections:

(A) – mechanical, (B) – control, (C) – measuring, (D) – auxiliary, and each of them consists of several basic elements, appropriately numbered.

This numbering is fully consistent with the structure diagram presented in Figure 2 (except for the omitted auxiliary section), facilitating understanding of the mutual functional relationships of the subsystems.

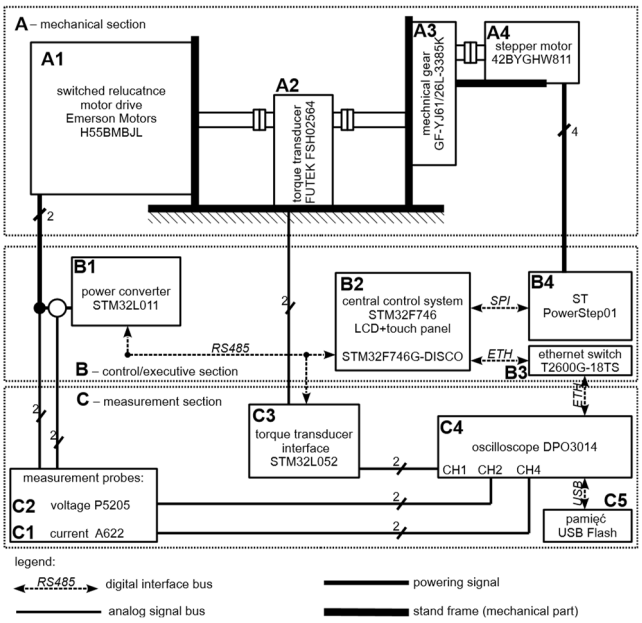

Fig. 2. Diagram of the structure of the laboratory station

The mechanical part consists of a kinematic chain connecting the tested motor (A1), a torque meter (A2), a mechanical transmission (A3), and a stepper motor (A4). This design enables precise rotation of the motor shaft in a very high resolution of 86,656,000 discrete positions without the need to use a position sensor (possible loss of synchronous motor operation is detected by the *PowerStep01* controller).

The control and executive part is mainly: a fully proprietary symmetrical converter (B1), and a central controller with a touch screen interface (B2) based on an evaluation board of an efficient STM32F series microcontroller with proprietary software enabling:

- distributed control of manual/automatic operation of the station,
- relatively quick/easy configuration of operating parameters via touch screen and a real-time status preview.

Elements: B3 (Ethernet switch) and B4 (stepper motor driver) are adapted factory designs.

Signal measurement/aggregation of:

- phase winding current i_p,
- excitation voltage U_p,
- generated torque T_p,

is carried out using standard probes: current - marked C1 (from drawings 1, 2), voltage (C2) and **author's torque meter interface** (C3). The signals are recorded by an oscilloscope (C4) and the appropriate acquisition time horizon is saved to a USB flash memory. The digital data saved in this way is transferred to a computing station (PC), read and processed in the Matlab environment (using proprietary scripts to automate processing) until the final result is obtained.

The acquisition process in the oscilloscope – like the entire process – can be controlled remotely and automatically (a separate section of this publication is devoted to this).

The auxiliary section consists of laboratory power supplies described as: *D*1 – powering converter supply, *D*2 – powering microelectronic systems.

More design and construction details regarding the stand, with particular emphasis on the original design of the converter (B1), are presented in the publications: [11] and [12]. The torque meter interface that determines the new functionality of the station in the context of the previously defined goal will be presented in the next section.

Torque meter interface

The main design consideration in determining the final solutions was to minimize interference in the measurement signal while maintaining the frequency band of the transducer itself. Hence, the structure was divided into two boards: the upper (digital) and the lower (analog), achieving a clear spatial separation of these two domains. Figure 3 shows the assembled real systems, and Figure 4 shows the solution for assembling both boards. The operating functional prototype is visible in the photo of the entire station (Figure 1).

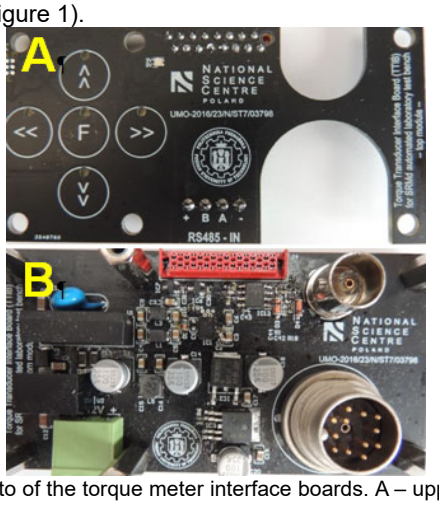

Fig. 3. Photo of the torque meter interface boards. A – upper one, B – lower.

Fig. 4. Design assembly of interface boards

The core of the digital board is the STM32L052 programmable unit. It is a relatively cheap IC matched with resources (flash memory, RAM, peripherals) to the planned functionalities:

- remote RS485 communication (peripherals: uart, dma),
- local communication (capacitive touch buttons),
- implementation of algorithms with limited complexity (e.g. auto-compensation of measurement offset).

The RS485 is galvanically separated to increase resistance to interference and to facilitate interface with bus nodes regardless of their power systems. The foundation of this solution in a proven system is presented in Figure 5. High-speed ISL8485ECBZ (up to 10 *Mbps*) was selected as RS485 transceiver. As in the galvanically separated bus, its power is supplied externally (by a so-called hybrid cable).

In terms of the local interface, the key aspect in designing the conductive fields of touch buttons is their appropriate size and appropriate separation from other signals.

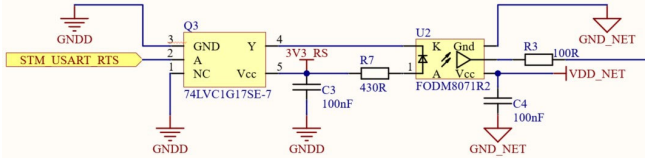

Fig. 5. System solutions for galvanic separation of the high data rate RS485 interface

The interface assumes capacitive fields with a diameter of 10 mm, the LED backlight is located at the edge of the field, and the signals are routed symmetrically from the source (differentially). Signalling in a range of capacitive fields should be avoided (at least limited) at all layers. The practical implementation of these postulates is shown in Figure 6. It should be also remembered to use an appropriate class of sampling capacitor in the peripheral system – preferably C0G (instead of e.g. the popular and cheap X5R/X7R) characterized by high temporal and thermal stability and high energy efficiency (in the design 10nF C0G was used). Using the above tips allows us to achieve a button status indicator separation in relation of 4-1.

Fig. 6. Touch fields design

Both the remote and local interface enable support for basic processing parameters of the torque value analog signal:

- change of gain,
- offset correction (signal zero adjustment).

The signal line between the board and the torque sensor is relatively long, so it is susceptible to interference. That is why the project provides two different powering sections:

a) remote Futek TRS705 transducer,
b) local analog signal processing path.

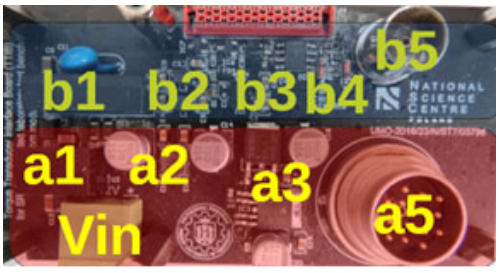

Fig. 7. Spatial distribution of subsystems of the analog interface processing path

As shown in Figure 8, both sections share a common voltage source of 12V (V_in) and the ground is only connected there. Next, the sections are galvanically separated, but in a similar order of individual components, i.e.:

(1) DC-DC impulse converter,
(2) a passive C-L-C filter with a passband well below the switching frequency range of the used converter,
(3) linear stabilizers of individual sections,
(4) chain of signal processing ICs,
(5) connectors (a5 – input – for torque meter, b5 – output – for oscilloscope).

In sensitive signal processing systems, attention should be paid to the noise parameters of each system element. In particular, the power supply parameters, the quality of which affects the operation of the entire system. Hence, a list of the linear stabilizers used and their noise parameters are presented in Table 1

Table 1.*SVR* – supply voltage rejection ratio, *eN* – output noise voltage.

SECTION	SYMBOL	V_{out}, SVR, eN
main track	LT3032EDE [13]	±12 V, 68 dB, 20 uV
transducer (A-part)	LF120ABDT [14]	+12 V, 82 dB, 50 uV
transducer (D-part)	LF50ABPT [14]	+5 V, 82 dB, 50 uV

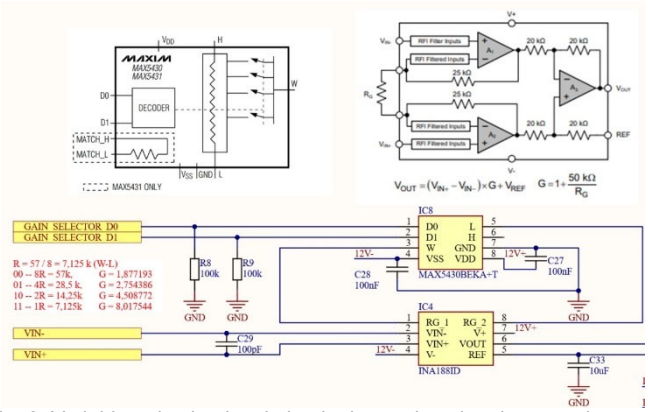

Fig. 8. Variable gain circuit solution in the analog signal processing path

The key signal processing solutions in the analog path look interesting. The functionality of gain change was achieved by connecting an instrumental amplifier with a programmable resistive ladder in the system as shown in Figure 8. The design challenge here is the need to obtain an agreement on the ranges of tolerated voltages and functional gain values (divider resistance). These difficulties were also revealed at the stage of solving the second key system, i.e. remote compensation of a constant shift in the measurement path. In this case, it is necessary to select a system that also guarantees an acceptable resolution. Most available digital potentiometer ICs operate at low voltages (up to 5 V) and are most often unipolar. The selected *AD*5200*BRMZ*50 [15] chip allows bipolar power supply, but ±2.5V . From the point of view of the implemented function, this is not a problem, because the required zero compensation range will not be too large. However, it is best if the power supply of the divider is shared with the power supply of the rest of the analog section (±12V). Unfortunately, the solution cannot be only a symmetrical separation of the resistance divider line from the higher voltage side because (according to the documentation) after resuming operation (before programming to the selected value), the ICs do not have both external interface electrodes connected, but only one. This requires protection against voltage breakdown of the system. According to the diagram in Figure 9, the system was expanded with the selected transil *PESD*2V 5Y 1*BSFY L* [16]. Before the offset finally reaches the instrumentation amplifier, the signal from the active electrode of the voltage divider is buffered in the *MCP*601*RT* operational amplifier circuit, passing through an R-C filter with a relatively high time constant (the stability of the offset is as important as the quality of the measurement signal). The output of the measurement signal after amplification, taking into account the programmed constant

shift, is buffered on the precision operational amplifier *OPA*202*IDBV R* [17] and finally reaches the BNC connector as an output for visualization/recording on an oscilloscope.

In the context of valuable functionality, the discussed interface – for internal purposes of controlling (programming) the research process – requires its measurement signal values. This is simply utilized by the use of an ADC converter, which is the peripheral of the microcontroller used.

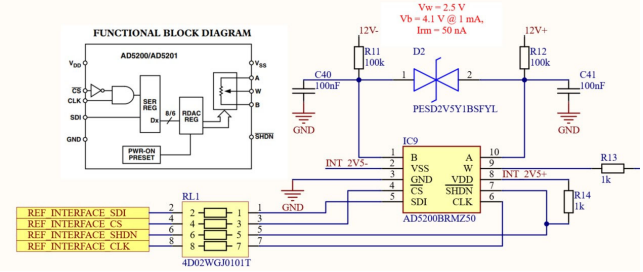

Fig. 9. Solution for selecting the shift of the constant value component in the measurement signal path

The permissible range of signal values in the analog path must be fit to MCU's voltage level before it is measured in the ADC buffer. This is done in the ideal rectifier system presented in Figure 10. Before being included in the electronic design, all subsystems were simulated and tested in the *LTSpice* environment (in the time and frequency domain). Hence, all the critical coefficients as:

- gain,
- input impedance,
- output impedance,
- step response,
- frequency response,

were determined to fit design requirements.

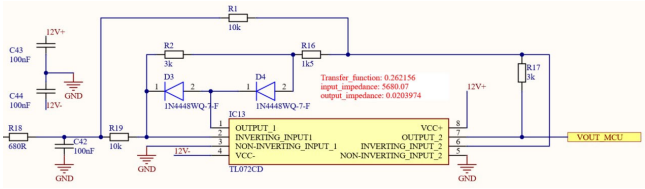

Fig. 10. Analog signal normalization path for conversion within the integrated ADC peripheral

Automatic zeroing of the measurement torque signal

One of the important software solutions implemented in the described system is automatic zeroing of the measurement signal. There is one difficulty resulting from this. Namely, the programmable unit (*STM*32*L*052), available remotely from the RS485 interface, cannot directly listen to the torque measurement line due to the voltage range mismatch. The use of an operational amplifier in an ideal rectifier system with a gain of k = 0,26 allows access to this information. The detailed solution was presented in the previous section of the publication, in Figure 10. The inevitable effect of this solution is the loss of information about the direction of the acting torque, and a certain non-linearity of the relationship will occur near zero value. Hence, a noise-resistant zeroing algorithm was developed. The operation consists of two main stages:

- preparation of measurement samples,
- statistical analysis of the collected data.

The algorithm of the first stage is presented in Figure 11. The simplification in the description lies in the fact that the measurement of the analog value itself, reduced to the *get_adc_meas*() instruction, actually consists of averaging 32 samples, each processed in a time interval of 10 miliseconds. The main parts of the algorithm consist of (section designations from Figure 11): A – zeroing measurement tables, used variables and setting the initial offset. B – due to the large time constant of the *offset* path, each change in its value must involve waiting 3 seconds for further instructions. The measurement is then run and its result (along with measurement with the associated offset value) is stored in an array. C: within this part, the auxiliary variable *dir* is used to verify whether the direction of change is correct, i.e. changing the offset reduces the value of the measured signal. If so, the algorithm moves to phase C. If not, the sweep direction changes with delta gain. If the change has the correct tendency, the transition to the D-part occurs (main and repeated one part of the algorithm). At constant time intervals with a constant change, subsequent pairs are registered: offset setting - processed value of the analog signal. Registration continues until the value memory size limit is reached or the initial value is obtained again. Obtaining any of these conditions causes the last pair to be saved and the statistics calculations to proceed.

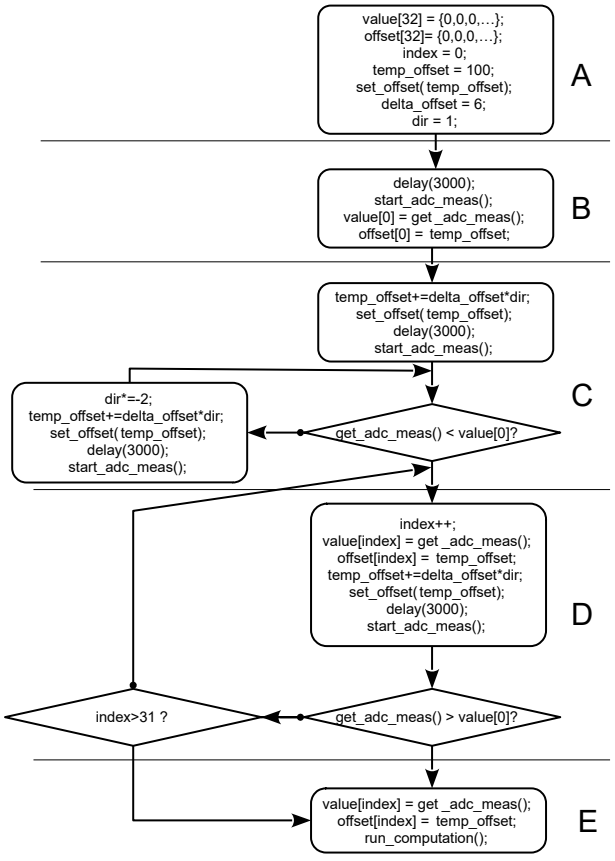

Fig. 11. Simplified algorithm for collecting data for signal zeroing

The input data for the calculations are measurement vectors (shift-measurement value pairs). From these pairs, the minimum value constituting the boundary between two groups of vectors with a monotonically decreasing value (G1) and an increasing value (G2) is searched for. These two groups are separately solved for linear regression parameters. To illustrate this, the figure 12 is zoomed in. The charts show sample measurements recorded in a real system.

Assuming the equation of a linear function:

$$y_i = a_i x + b_i \tag{13}$$

the algorithm solve two regressions, where i = 1 – decreasing function (G1 group), i = 2 – increasing function (G2):

(14) $$x = \frac{b_2 - b_1}{a_1 - a_2}.$$

The solutions are shown in the figures with dashed vertical lines. The improved version of the algorithm rejects measurements that deviate from expected (potentially disturbed) measurements. This is done in such a way that for the determined linear regression, all measurement points are examined for the difference from the expected value, the calculation of which comes down to the use of the formula:

(15) $$\sigma^2 = \sum_{i=0}^{N} \frac{((ax_i + b) - y_i(x_i))^2}{N},$$

where: σ^2 – variance, N – number of measurement vectors a – slope coefficient of regression, b – regression shift, $(y_i;x_i)$ – a set of indexed measurement vectors i.

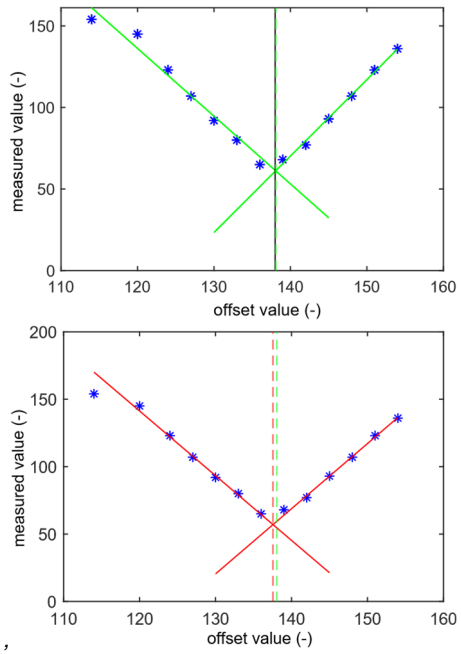

Fig. 12. The result of the zeroing algorithm in two versions: original (without statistical elimination of measurement points - upper graph) and corrected (lower graph)

If the square of the difference between the expected and measured values at a given point is greater than the regression variance, this measurement point is rejected from the set and the regression coefficients and variances are recalculated (which is an indicator of the quality of fit). In terms of this variance indicator, the following sets are compared:

- starting point sets,
- sets cleaned of points far from expected,
- sets cleared one by one from each of the points originally marked for removal.

Data sets are considered valid for the lowest obtained value of the fit quality coefficient for the above combinations. As shown in the example, the modified version produced slightly different results and was the best in experiments. The difference in the example is shown in Figure 12 (bottom graph), which, in addition to the best solution (red dashed line), shows the solution without taking into account the statistical quality of the measurement points (green line).

The algorithms were migrated from the *Matlab* test environment to the *STM32L052* embedded system program in stages, with the structure and naming of functions consistent for both environments. This enabled a relatively quick verification of the correctness of the results obtained. Despite differences in number formats precision (in Matlab - double precision, for the STM32 system a combination of an integer type with single-precision floating-point encoding, i.e. *float* type), the intermediate and final results did not differ by more than 1%.

The graphs in Figures 13 and 14 present exemplary, experimental operation of the algorithm for zeroing the measurement value (the entire process and the effect of operation on the changed scale, respectively). The series connection of the R1-R2-R3 resistor system (100k-50k-100k) appropriate for the offset compensation execution path, with ±12 V power supply and 8-bit resolution of the digital setting allows for obtaining an elementary offset correction Δ_o in accordance with by the formula of 18 mV :

(16) $$\Delta_o = \frac{R_2(V_{cc} - V_{ee})}{(R_1 + R_2) \cdot 2^k} = \frac{50(12+12)}{200 \cdot 2^8} = 0{,}018 .$$

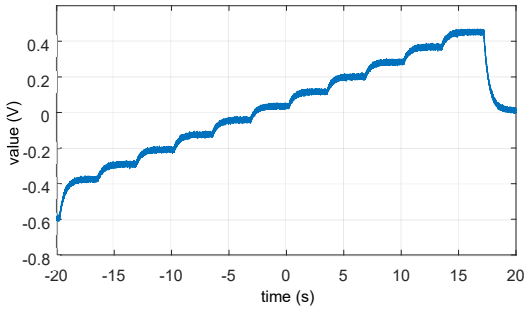

Fig. 13. Progress of the measured value during the zeroing process

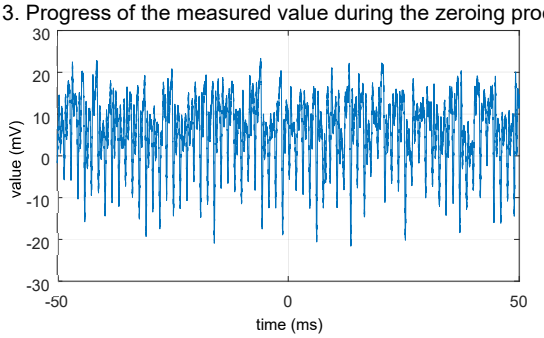

Fig. 14. The waveform of the measured value – the effect of the measurement zeroing process

Hence, if the average value of the measurement acquisition after the zeroing process is in the range ±9 mV , it can be considered as the best possible offset match. The signal value after running the zeroing process in several repetitions is listed in the table . The results show that the correct final result was obtained in each of the tested runs.

Results of operation

An example of the effect of aggregation of raw measurement data (phase current i_p and the corresponding value of the generated electromagnetic moment T_p at a given position θ_p) during automatic operation of the station is presented in Figure 15.

Table 2. Summary of the calculated average values of the resulting waveforms for 4 repetitions of the measurement signal zeroing algorithm

it.	value (mV)	in range
1	6,82	YES
2	5,66	YES
3	6,03	YES

4	6,10	YES

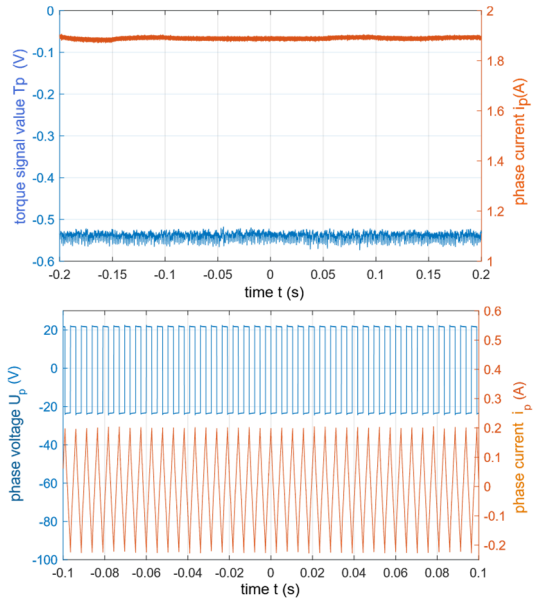

Fig. 15. Examples of raw measurement data for two different converter control modes. HF mode (top), LF mode (bottom).

These data were obtained as a result of the implementation of programmed operations (specific to the automatic operation mode of the station):

1. low-frequency operation forcing with peak-to-peak current control, acquisition of excitation voltage and current response (to determine the inductance in a given position θ_p),
2. reconfiguration of the converter for high-frequency operation with current regulation at a given value, preparation for the acquisition of torque and phase current measurement (remote reconfiguration of the oscilloscope),
3. performing a series of measurements within a predefined range i_{pMIN} to i_{pMAX} in the number of k measurement points,
4. moving the shaft to a new position by $\Delta\theta_p$. Importantly, during the implementation of the above operations, open interfaces of the nodes of the distributed control system and the implementation of the new DPO3014 oscilloscope control protocol allowed for (in real-time):

- selection of the scale on the current measurement channel (the current-torque relationship in a switched reluctance motor is quadratic),
- adjusting the time base to obtain a similar number of PWM forcing cycles regardless of the band inductance change (with moving motor shaft θ_p),
- selection of channels on which the acquisition takes place (a different set of signals is used to measure inductance than to measure the torque-current relation-
  ship),
- selection of the reference position of the waveforms to ensure good coverage of the measurement range (in the middle of the oscilloscope screen when symmetric, bipolar phase excitation is used and in the bottom at unipolar one).

Figures 16 and 17 visualize the result of the process of examining the relationship between the electromagnetic torque generated in the motor and two variables: rotor position angle θ_p and the phase winding current i_p. The assumed values of the electromagnetic torque at given points are the result of averaging the waveform values as in the example 15 and computation according to the following formula (taking into account the gain of the analog interface and the parameters of the torque transducer):

$$T_p = \frac{T_{pv} D_R}{D_V k_A} = T_{pv} \frac{5}{5 \cdot 1{,}877} \quad , \tag{17}$$

where: T_p (Nm) – the resulting torque value, T_{pv} (V) – measured voltage value of the torque signal, D_R (Nm) – measuring range of the torque sensor, D_V (V) – voltage value corresponding to the measurement range, k_A (V/V) – signal amplification of the measurement interface.

The obtained results show the expected relationships (e.g. quadratic dependence of the torque value on the phase current). The shapes of the presented relationship in the negative and positive parts are symmetrical.

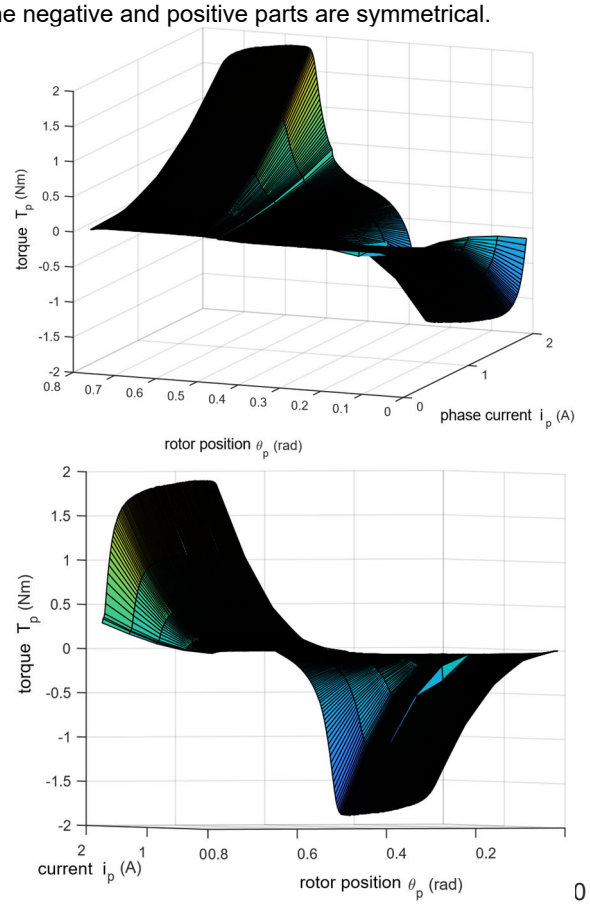

Fig. 16. The result of processing data collected in automatic mode – selected isometric projections of the relationship $T_p = f(\theta_p, i_p)$

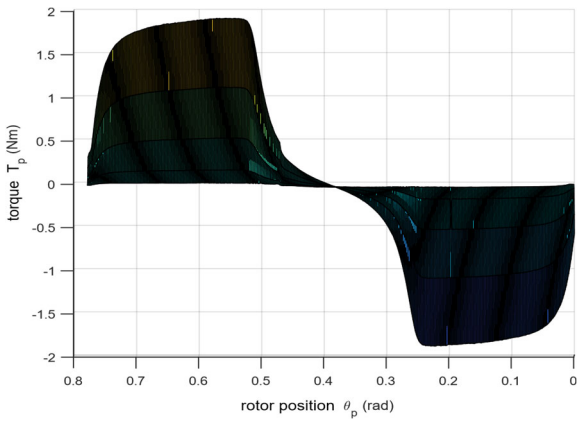

Fig. 17. The result of the acquisition in automatic mode – relationship view of $T_p = f(\theta_p)$

Summary

The article presents selected solutions of the author's laboratory test-bench for testing a switched reluctance motor drive. The introduction presents fundamental formulas constituting the analytical basis (motivation) for the development of the research stand and the direction of the work being carried out. The structure of the test bench was presented as clearly as possible, thus complementing previous publications on the topic. Attention was focused in particular on the newly developed interface of the Futek TRS705 flythrough torque meter, which discussed hardware solutions enabling obtaining a high-class measurement signal with the possibility of: changing the gain and zeroing in the analog signal trace. For this second functionality, the implemented algorithm and the results are described, which turned out to meet the assumed accuracy conditions. To confirm the consistency of the proposed structure and its functionality, the first results of data aggregation in a full, automatic measurement cycle intensively using communication on shared, open interfaces were presented. The aggregation of measurement data turned out to be repeatable and consistent with the planned program, as evidenced by an example set of data collected from 420 positions for 5 different phase current excitations. Among this set, only one false measurement was identified, which can be filtered out at the secondary processing stage. The collected data on various process parameters will constitute the basis for the development of analytical reference models used for advanced control purposes. It should be noted that the tasks of fault-tolerant control or those aimed at reducing torque pulsations in a switched reluctance drive are still the subject of intensive research [18], [19].

Solutions that go beyond the adopted topic of the study (implementation of a new oscilloscope control protocol, and data exchange architecture within the multi-threaded central controller system) will be the subject of a separate publication. Materials demonstrating the operation of the station, which supplement the publication, are available at [20].

The article was written with the support of the Polish National Science Center (NCN, ncn.gov.pl) as a result of grant titled „Nonlinear reference model in fault tolerant control of the switched reluctance motor drive" based on the agreement UMO-2016/23/N/ST7/03798.

REFERENCES

[1] R. Krishnan, "Switched Reluctance Motor Drives: Modeling, Simulation, Analysis, Design, and Applications". CRC Press, Dec. 2017, google-Books-ID: plBgngEACAAJ.

[2] P. Bogusz, M. Korkosz, A. Mazurkiewicz, and J. Prokop, "Modelowanie maszyny SRM jako układu o zmiennych indukcyjnościach przy użyciu programu PSpice", *Prace Naukowe Instytutu Maszyn, Napędów i Pomiarów Elektrycznych Politechniki Wrocławskiej. Studia i Materiały*, vol. 66, no. nr 32, t. 1, pp. 196–202, 2012

[3] J. Prokop and P. Bogusz, "Analiza właściwości dynamicznych silników reluktancyjnych przełączalnych w systemie MATLAB/SIMULINK", *Przegląd Elektrotechniczny*, vol. nr 5, pp. 119–124, 2000

[4] A. Maciejuk and J. Deskur, "Simple Models of Switched Reluctance Motors for Fast Simulation and Real-Time Control Application", EPNC 2004: 18 Symposium, Poznań, Poland, June 28-30, 2004

[5] B. Fabianski and K. Zawirski, "Parameter adaptation of simplified switched reluctance motor model using Newton and GaussNewton signal fitting methods", *COMPEL - The international journal for computation and mathematics in electrical and electronic engineering*, vol. 36, no. 3, pp. 602–618, 2017

[6] B. Fabiański and K. Zawirski, "Simplified model of Switched Reluctance Motor for real-time calculations", *Przegląd Elektrotechniczny*, vol. R. 92, nr 7, 2016

[7] I. Husain and S. Hossain, "Modeling, Simulation, and control of switched reluctance motor drives", *IEEE Transactions on Industrial Electronics*, vol. 52, no. 6, pp. 1625–1634, Dec. 2005, conference Name: IEEE Transactions on Industrial Electronics.

[8] J. Prokop, "Kompleksowe modelowanie silników reluktancyjnych przełączalnych w systemie MATLAB/MAPLE", *Przegląd Elektrotechniczny*, vol. R. 77, nr 7-8, pp. 191–196, 2001

[9] M. Kowol, P. Mynarek, and D. Mroczen, "Model matematyczny przełączalnego silnika reluktancyjnego do analizy stanów dynamicznych", *Maszyny Elektryczne: zeszyty problemowe*, vol. Nr 88, pp. 7–11, 2010

[10] "Non-Contact Shaft-to-Shaft Rotary Torque Sensor with Encoder TRS705 : FSH02564." [Online]. Available: https://www.futek.com/store/torque-sensors/shaft-to-shaftrotary-torque-sensors/non-contact-shaft-to-shaft-rotaryencoder-TRS705/FSH02564

[11] B. Fabiański, K. Zawirski, and T. Pajchrowski, "Zautomatyzowane stanowisko laboratoryjne do precyzyjnego wyznaczania kątowego rozkładu indukcyjności uzwojenia pasma silnika reluktancyjnego przełączalnego" *Przegląd Elektrotechniczny*, vol. 99, no. 5, pp. 161 – 170, 2023

[12] T. Pajchrowski, B. Fabiański, and K. Zawirski, "Precyzyjne wyznaczanie rozkładu kątowego indukcyjności uzwojenia silnika reluktancyjnego przełączalnego z wykorzystaniem dedykowanego, zautomatyzowanego stanowiska laboratoryjnego", *Przegląd Elektrotechniczny*, vol. 99, no. 5, pp. 177 – 183, 2023

[13] "LT3032 Series - Dual 150mA Positive/Negative Low Noise Low Dropout Linear Regulator"

[14] "LFXX-Very lowdrop voltage regulator with inhibit - STM." [Online]. Available: https://www.st.com/en/power-management/lfxx.html

[15] "AD5200 Datasheet and Product Info | Analog Devices." [Online]. Available: https://www.analog.com/en/products/ad5200. html

[16] "PESD2V5Y1BSF - Extremely low capacitance bidirectional ESD protection diode." [Online]. Available: https://www.nexperia.com/product/PESD2V5Y1BSF

[17] "OPA202 | Buy TI Parts | TI.com." [Online]. Available: https://www.ti.com/product/OPA202/part-details/OPA202IDBVR

[18] Z. Xia, G. Fang, D. Xiao, A. Emadi, and B. Bilgin, "An Online Torque Sharing Function Method Involving Current Dynamics for Switched Reluctance Motor Drives," *IEEE Transactions on Transportation Electrification*, vol. 9, no. 1, pp. 534–548, Mar. 2023, conference Name: IEEE Transactions on Transportation Electrification.

[19] X. Sun, X. Tang, X. Tian, G. Lei, Y. Guo, and J. Zhu, "Sensorless Control With Fault-Tolerant Ability for Switched Reluctance Motors," *IEEE Transactions on Energy Conversion*, vol. 37, no. 2, pp. 1272–1281, Jun. 2022, conference Name: IEEE Transactions on Energy Conversion

[20] "SRMd – google drive." [Online]. Available: https://drive.google.com/drive/folders/1RyXi_ h28BUn5Heiu7-rvqOtmGngrjEuK?hl=pl